ELSEVIER

International Journal of Heat and Fluid Flow 22 (2001) 543–551

International Journal of HEAT AND FLUID FLOW

www.elsevier.com/locate/ijhff

Bubble motion during inclined intermittent flow

M. Cook, M. Behnia *

School of Mechanical and Manufacturing Engineering, University of New South Wales, Sydney, NSW 2052, Australia

Received 27 June 2000; accepted 13 March 2001

Abstract

An experimental and numerical study of the motion of bubbles in inclined intermittent gas–liquid flow has been performed. A knowledge of the velocity of bubbles is critical to the determination of the pressure drop and heat transfer characteristics in such flows. Measurements show a transition in the dynamics of the bubble at a critical flow rate and this critical point has been shown to be related to the drift velocity of a bubble in a stagnant liquid. A numerical investigation of bubble drift in stagnant liquids has been performed with the use of the Volume of Fluid (VOF) technique. The results of the computations are shown to depend on the phase interface to wall contact angle, however, with a suitable choice of this parameter the calculated bubble motion matches well with the measured data. The bubble interface shape is also compared against data obtained with the use of a parallel wire conductance probe to further validate the computational results. © 2001 Elsevier Science Inc. All rights reserved.

Keywords: Bubble; Two-phase; Volume of Fluid; Intermittent flow; Slug

1. Introduction

The motion of bubbles in a flowing liquid commonly occurs in many industrial flow situations such as the production of steam and water in geothermal and conventional thermal power plants, refrigeration equipment and the core cooling of nuclear reactors, with the largest bubbles occurring during intermittent gas–liquid flows. This flow pattern occurs when waves of a stratified liquid layer grow to reach the top of the pipe and the gas propels a 'slug' of liquid along the pipe. The resulting flow pattern consists of a series of liquid slugs separated by bubbles that occupy almost the entire pipe cross-section. Under some flow conditions the bubbles may be well-formed Taylor type bubbles, however, at high flows they can deviate from this shape with the front of the bubble centred within the pipe (Bendiksen, 1984).

At non-zero inclinations intermittent flows are especially common as the liquid is unable to remain stratified under such conditions. Many applications involve flows inclined between the horizontal and vertical and the drift velocity of bubbles has been shown to behave quite strangely with changes in inclination. Bonnecaze et al. (1971) were the first to explain the observed maximum drift velocity of Taylor bubbles at intermediate inclination angles. They reasoned that the velocity along the bubble interface streamline is proportional to the vertical distance from the stagnation point at the bubble nose. Further, as the tube is declined from the vertical this distance first increases and then decreases as the inclination is lowered. This gives a qualitative explanation, however, no successful attempt has been made to quantify the bubble velocity as a function of inclination angle.

Bendiksen (1984) has proposed a simple correlation for the inclined bubble drift velocity based on the drift velocity in both horizontal and vertical configurations. The velocity of Taylor bubbles in vertical and horizontal pipes has been derived analytically for potential flow and the effect of surface tension has been studied experimentally by Zukoski (1966). Dumitrescu (1943) and Davies and Taylor (1950) were the progenitors of bubble rise theory in pipes, both applying potential flow theory to the calculation of flow around the front of a vertical bubble. The existence of a drift velocity component of bubbles in a horizontal pipe during two-phase flow is less obvious. Some experimental investigators such as Dukler and Hubbard (1975) and Heywood and Richardson (1979) found that their bubble velocity data did extend to zero as the flow velocity was decreased. The data of Mattar and Gregory (1974) and others, however, shows that a non-zero horizontal drift velocity does exist. Benjamin (1968) applied inviscid flow theory to the problem of a bubble penetrating into a horizontal pipe opened at one end and the resulting horizontal velocity compared well with the drift data collected by Zukoski (1966). The literature concerning the motion of bubbles in intermittent flows has been summarized well by Fabre and Line (1992).

Recently, a number of computational studies have been performed to simulate bubble motion in pipes such as the work of Clarke and Issa (1997), Tomiyama et al. (1994), Rudman (1998) and Mack et al. (1997). All these have been limited to vertical flow, channel flow or zero gravity conditions where symmetry can be exploited.

* Corresponding author. Tel. +61-2-9385-4253; fax: +61-2-9663-1222.
E-mail address: m.behnia@unsw.edu.au (M. Behnia).

0142-727X/01/$ - see front matter © 2001 Elsevier Science Inc. All rights reserved.
PII: S0142-727X(01)00113-8

Notations

C	bubble velocity proportionality constant
D	diameter
Fr	Froude number
g	gravitational acceleration
n	unit normal vector
t	time
u	velocity in x direction
U_d	drift velocity
v	velocity in y direction
V_B	bubble velocity
V_T	slug translational velocity
w	velocity in z direction
x	axial direction
y	transverse direction
z	vertical direction
β	inclination angle to the horizontal
Δ	change in
ϑ	volume fraction
Σ	dimensionless surface tension
K	interface curvature
ϕ	wall contact angle
μ	dynamic viscosity
ρ	density
σ	surface tension coefficient

2. Bubble velocity in a flowing liquid

Measurement of bubble velocity was undertaken in two pipes of 32 mm and 50 diameter that could be inclined to +10° with air and water used as the two phases. Bubble velocity was measured with conductance electrodes that served as triggers to identify the front and rear of individual bubbles, as described in Cook and Behnia (2000). The sampling rate was adjusted to ensure that the error in the calculated velocity was less than 3%. Additionally, the velocity of many bubbles was averaged to further reduce the error. The flow rate of both phases was metered accurately and gas expansion effects were accounted for by measuring the local static pressure at the test section where measurements were taken. Bubble velocity data was obtained for both continuous intermittent flow and for individual bubbles injected into the liquid flow, for a range of overlapping flow rates, and no significant difference in the bubble velocity data was detected.

The measured values of the bubble translational velocity as a function of the flow mixture velocity are shown graphically in Figs. 1–3 for both the 32 and 50 mm diameter pipes. It can be readily seen that at each angle of inclination two separate regions exist, for low flows the bubble velocity increases relatively slowly with an increase in flow velocity, until a transition occurs after which the bubble velocity increases more quickly with mixture velocity. In both regions the bubble velocity varies linearly with mixture velocity and can be expressed as

$$V_T = CV_m + U_d, \tag{1}$$

where U_d is the drift velocity in a stagnant liquid.

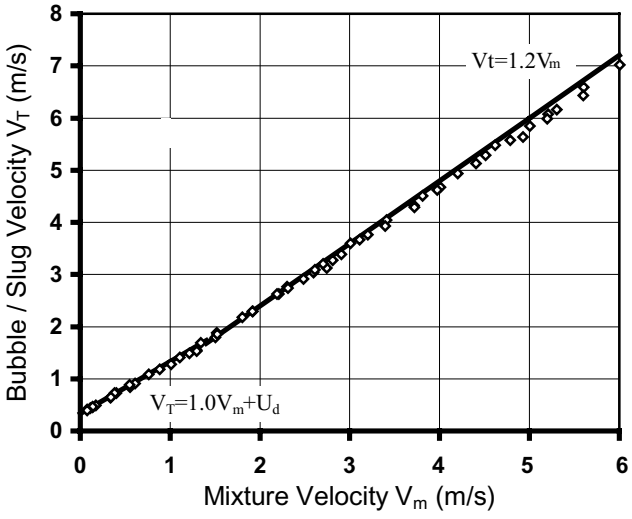

Fig. 2. Bubble velocity vs mixture velocity ($\beta = +5°$, $D = 50$ mm).

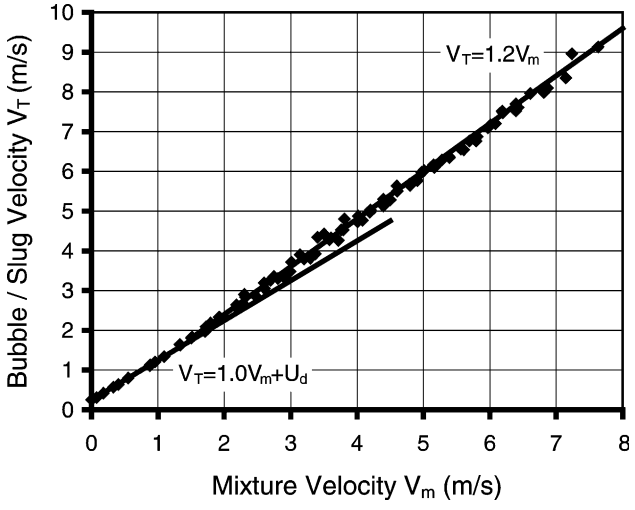

Fig. 1. Bubble velocity vs mixture velocity ($\beta = +5$, $D = 32$ mm).

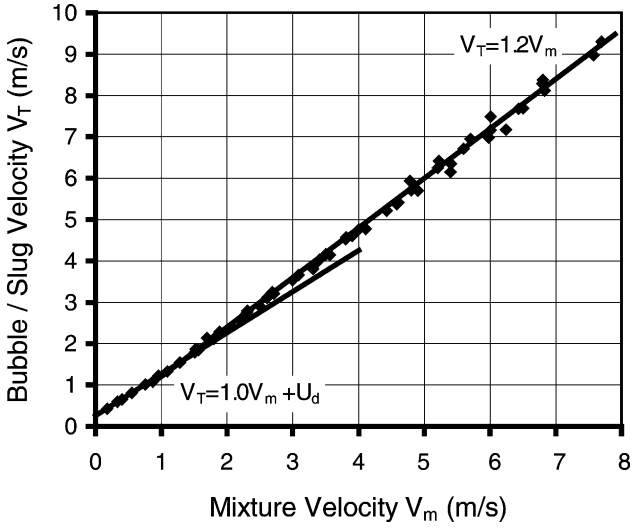

Fig. 3. Bubble velocity vs mixture velocity ($\beta = +10°$, $D = 32$ mm).

Bendiksen (1984) and Ferre (1979) have both observed transitions similar to those observed here, however, Ferre found two transitions at mixture Froude numbers of $Fr_m = 2.0$ and 8.0, where

$$Fr_m = \frac{V_m}{\sqrt{\frac{\Delta\rho}{\rho_L} gD}}. \quad (2)$$

Bendiksen suggests that transition occurs at $Fr_m = 3.5$ for all pipe diameters and inclinations. Additionally, the distribution parameter, C, in Eq. (1) was found to have a constant value of 1.05 by Bendiksen, while Ferre observed a value of 1.1 and Singh and Griffith (1970) report a value of 0.95.

The data displayed in Figs. 1–3 show a number of interesting features. First, at velocities above the transition value the bubble velocity is unaffected by any drift velocity component and the velocity is accurately correlated by $V_T = 1.2\ V_m$, for both the horizontal and inclined cases. This is consistent with Bendiksen's observation that at the critical Froude number, the radial bubble nose position moves towards the pipe centreline and the bubble propagation rate is controlled by the local liquid velocity at its tip. Assuming a developed velocity profile in the liquid ahead of the bubble then this velocity will be close to 1.2 times the flow mixture velocity for turbulent flows.

For flows below the critical value the bubble velocity was found to depend on both the pipe diameter and inclination angle. For the 32 mm diameter pipe, the data is best fitted by a value of 1.0 for C with U_d found by extrapolating the data to zero flow rate. The 50 mm diameter pipe data yielded a value closer to $C = 0.95$. Bendiksen (1984) found that the transition occurred in stages, however, no evidence for this can be seen in the data here.

The present data also suggests that the forces controlling the bubble propagation rate alter quite suddenly at the critical mixture Froude number. Below this flow rate the bubble appears to be controlled by buoyancy forces, with its velocity approximately equal to the drift velocity in a stagnant liquid, plus the average flow velocity. Above the critical mixture velocity, the bubble is pulled along by the maximum liquid velocity ahead of the bubble nose. The data shows that the transition Froude number is not constant, as suggested by Bendiksen (1984) and Ferre (1979), but increases with inclination angle as the drift component increases. Paglianti et al. (1996) conducted air–oil experiments and concluded that the critical Froude number also depends on the properties of the fluids used. Further, the results show that transition occurs at considerably lower flows than suggested by Bendiksen (1984), whose correlation implies transition at a mixture velocity of 2.45 m/s in the 50 mm diameter pipe, which is almost twice the value found in the results presented here. The discrepancy between the 32 mm data and Bendiksen's correlation is less significant, which is not surprising as Bendiksen's results are based on air–water data collected in 19 and 24 mm diameter tubes. This indicates that specifying transition at a set Froude number is not sufficient for all pipe diameters and inclinations, and that the transition velocity for any pipe diameter and inclination is dependant on the bubble drift velocity.

The following more general correlation is proposed for the bubble/slug velocity at all flow rates at low to moderate inclinations, and is expected to be sufficiently accurate for engineering calculations.

$$V_T = \max \left\{ \begin{matrix} 1.0V_m + U_d \\ 1.2V_m \end{matrix} \right\}. \quad (3)$$

The correlation proposed above implies that transition occurs at

$$V_m = 5.0U_d, \quad (4)$$

which is in good agreement with the data shown in Figs. 1–3.

2.1. Identification of intermittent flow sub-regimes

Most investigators of intermittent two phase flows such as Paglianti et al. (1996), Gregory et al. (1978) and Kokal and Stanislav (1989) have noted that many flow properties exhibit very different characteristics depending on the total superficial flow velocity. Generally, a distinction between elongated bubble flow, that occurs at low velocities, and slug flow, occurring at high velocities is made. Elongated bubble flow is more prevalent in large diameter oil field pipelines and is characterised by slow well-formed bubbles moving between relatively unaerated slugs producing a relatively low pressure gradient. Slug flow, however, is distinguished by a pronounced mixing vortex at the front of the slug and consequent aeration of the slug body. Interestingly, Fagundes-Netto et al. (1999) have characterised the different regimes by the existence of an abrupt or gradual rise in the liquid level behind the bubble. Intermittent flow models need to correctly account for the discontinuity in the various flow properties at the transition between these sub-regimes if accurate modelling over the whole intermittent regime is to be achieved.

The bubble velocity results of this section suggest that the distinction between the flow sub-regimes is produced by the change in bubble dynamics. That is, above the transition velocity the fluid at the pipe centre moves at 1.2 times the mixture velocity. If the bubble and slug were to move slower than this value, it would imply the unrealistic situation that the fluid at the centreline moves forward within the slug. At transition the bubble nose moves from the top of the pipe to the pipe centreline, as observed by Bendiksen (1984), and the bubble/slug speed increases relative to the liquid film ahead of the slug. This results in the development of the mixing vortex producing the longer and more aerated slugs that are characteristic of slug flow. Examination of Fig. 4 shows that the void fraction of the slug body does indeed rapidly increase for mixture velocities greater than the transition velocity defined in Eq. (4). Measurements of slug holdup were made with a parallel wire conductance probe as described in Cook and Behnia (1997).

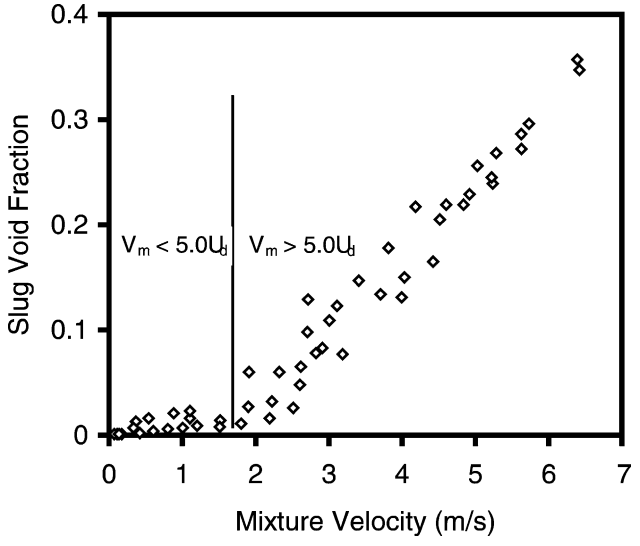

Fig. 4. Slug void fraction increase at transition ($\beta = +10°$, $D = 50$ mm).

Similar results were obtained at all angles of inclination and for both pipe diameters.

Clearly, the transition in the velocity of the bubble and slug unit proposed here in Eqs. (3) and (4) has implications for all the flow parameters, and appears to accurately define and distinguish between the elongated bubble and slug flow subregimes. The transition velocity is therefore very important in the modelling of intermittent flow and as a consequence, knowledge of the bubble drift velocity, on which the transition depends, is necessary. Numerical and experimental investigations of the bubble drift velocity are the subject of the following sections.

3. Measurements of bubble drift velocity

The 32 and 50 mm diameter pipes attached to the inclinable flow rig were filled with water and the return valve shut so as to enable measurement of the velocity of long bubbles in a stagnant liquid. Single bubbles were injected into the pipes with the use of the solenoid valve attached to the gas circuit and the bubble velocities were measured with the conductance probes. Bubbles of various lengths were obtained by altering the time the solenoid valve remained open, and the length of the bubble was found to have no effect on the observed velocity. The effect of fluid properties on the terminal bubble rise velocity was investigated by filling the 50 mm acrylic pipe with ethylene glycol and the shape of a rising bubble was also measured during these experiments by collecting the voltage output from the parallel wire conductance probe. At any combination of inclination, diameter and fluid properties at least 10 bubble speeds were measured and the spread of results was consistently less than 1%.

The 16 m long rig was limited to a maximum angle of inclination of $+10°$, however, such a long pipe was not required for the current series of experiments. So a new rig was employed to facilitate bubble drift velocity measurements at all angles of inclination. This rig could be inclined from horizontal to vertical in 15° increments and was designed to hold a polycarbonate pipe of 2.9 m in length and 44.5 mm internal diameter.

The data of Zukoski (1966) stand as the pre-eminent experimental work on inclined bubble motion and Zukoski's results show that the bubble Froude number defined by

$$Fr_B = \frac{V_B}{\sqrt{(\Delta\rho/\rho)gD}} \tag{5}$$

is determined almost solely by the inclination angle and the dimensionless surface tension defined by

$$\Sigma = \frac{\sigma}{\Delta\rho g D^2}. \tag{6}$$

The three pipe diameters and two liquids used here allowed dimensionless surface tensions over the range 17.5×10^{-4} to 7.4×10^{-3} to be examined. The large difference in density between the liquid and gas phase meant the variation in the air bubble density resulting from the reduction in pressure head as the bubble rose, was not significant. The liquid properties are the significant quantities and the nominal values are given below.

Water@20°C	$\rho = 998.2$ (kg/m^3)	$\sigma = 7.36 \times 10^{-2}$ (N/m)	$\mu = 0.001$ (kg/m.s)
Ethylene glycol@20°C	$\rho = 1113$ (kg/m^3)	$\sigma = 4.8 \times 10^{-2}$ (N/m)	$\mu = 0.021$ (kg/m.s)

The experimental results are summarised in Table 1. Good agreement was found between the data collected in the present experiments and those of Zukoski. Notably, all the results show that the maximum drift velocity is attained at inclinations between 30° and 45°.

4. Numerical simulation of bubble motion

A computational study of the drift of bubbles was conducted in an attempt to remove the empiricism from the determination of bubble drift velocity currently necessary when applying intermittent flow models.

4.1. Numerical method

The effect of surface tension and tube inclination on the rise velocity of a 3D bubble was modelled using a commercially available computational fluid dynamics code. The interaction of the immiscible gas and liquid phases was modelled with the Volume of Fluid (VOF) algorithm of Hirt and Nichols (1981). Rather than solving separate conservation equations for each phase, the VOF technique requires only a single set of equations common to both phases to be solved, and the resulting velocity field is shared between the phases. The transient Cartesian mass and momentum conservation equations are given by:

$$(\text{continuity})\ \frac{\partial\rho}{\partial t} + \frac{\partial(\rho u)}{\partial x} + \frac{\partial(\rho v)}{\partial y} + \frac{\partial(\rho w)}{\partial z} = 0, \tag{7}$$

Table 1
Inclined bubble rise velocity results

Case	D (mm)	β(°)	Liquid	$\Sigma(\times 10^{-3})$	V_B (m/s)	Fr_B
1	32.0	5.0	Water	7.4	0.251	0.448
2	32.0	10.0	Water	7.4	0.262	0.468
3	50.0	5.0	Water	3.0	0.337	0.481
4	50.0	10.0	Water	3.0	0.350	0.50
5	50.0	5.0	Ethel. G.	1.75	0.335	0.479
6	50.0	10.0	Ethel. G.	1.75	0.346	0.494
7	44.5	15	Water	3.8	0.338	0.512
8	44.5	30	Water	3.8	0.359	0.544
9	44.5	45	Water	3.8	0.370	0.560
10	44.5	60	Water	3.8	0.339	0.513
11	44.5	75	Water	3.8	0.286	0.433
12	44.5	90	Water	3.8	0.229	0.347

$$(x\text{ momentum})\frac{\partial(\rho u)}{\partial t}+\frac{\partial(\rho uu)}{\partial x}+\frac{\partial(\rho vu)}{\partial y}+\frac{\partial(\rho wu)}{\partial z}$$
$$=-\frac{\partial P}{\partial x}+\frac{\partial}{\partial x}\left[\mu\frac{\partial u}{\partial x}\right]+\frac{\partial}{\partial y}\left[\mu\frac{\partial u}{\partial y}\right]$$
$$+\frac{\partial}{\partial z}\left[\mu\frac{\partial u}{\partial z}\right]+\rho g_x+F_x. \quad (8)$$

The y and z momentum equations are similar to Eq. (8) and for the sake of brevity are not shown. The last two terms in Eq. (8) are body force terms, the first of these represents the directional component of gravitational force and the last term is an additional force term that results from interfacial surface tension. The finite volume technique was used to solve the governing equations on a structured grid. The equations are discretized by integrating about each control volume, yielding finite difference equations that conserve each quantity, mass and momentum, over each control volume.

In Eqs. (7) and (8), the fluid properties are written as dependant variables despite calculations being performed for incompressible laminar flow. Additionally, the equations involve only one value of each of the fluid properties of density and viscosity despite the use of these equations to solve the flow field common to both phases. The value of each property used in each control volume is determined by the following relations:

$$\rho=(1-\vartheta)\rho_1+\vartheta\rho_2 \quad (9)$$

and

$$\mu=(1-\vartheta)\mu_1+\vartheta\mu_2, \quad (10)$$

where ϑ is an additional variable introduced as part of the VOF technique and is referred to as the volume fraction of the secondary phase. Thus the property values used in each control volume calculation are a weighted average of the single phase properties and vary in both space and time. For the two-phase problem modelled here, only one volume fraction is defined with $0\leqslant\vartheta\leqslant 1$, and the gas–liquid interface exists in a control volume whose value of ϑ lies between 0 and 1. The volume fraction must satisfy a continuity requirement given by Eq. (11) and the interface motion is tracked by the solution to this closure equation giving the evolution of the ϑ field.

$$\frac{\partial\vartheta}{\partial t}+\frac{\partial(\vartheta u)}{\partial x}+\frac{\partial(\vartheta v)}{\partial y}+\frac{\partial(\vartheta w)}{\partial z}=0. \quad (11)$$

The VOF formulation requires special treatment for the interpolation of volume fraction fluxes across control volume faces near the interface. The finite volume solution technique requires fluxes of each variable across control volume faces to be calculated and balanced with source terms within the control volume itself. In this work, both the power-law and a second-order-upwind scheme were employed to interpolate face fluxes from neighbouring control volume values, and no significant difference between the respective solutions was found. When a cell is near an interface and $0<\vartheta<1$, special care is taken in the calculation of the volume fraction fluxes to avoid numerical diffusion and preserve a sharp definition of the phase interface. The method employed by the VOF technique is a 'donor–acceptor' flux approximation whereby each cell and its immediate neighbour is identified as either a donor of volume fraction or an acceptor of the same amount of volume fraction. The amount of fluid convected across a cell boundary is determined by the gradient of the volume fraction within each neighbouring cell. From this an estimate of the interface shape is made and used in the computation of the flux (Hirt and Nichols, 1981).

The effect of surface tension was modelled using the continuum surface force model of Brackbill et al. (1992). This model interprets surface tension as a continuous, 3D effect across an interface rather than as a boundary value condition at the interface. The change in pressure between two fluids across an interface is a function of the surface tension coefficient and the local curvature of the interface. In the model of Brackbill et al. (1992), the interface curvature is found from the volume fraction field. The normal to the interface is given by the gradient of the volume fraction field:

$$n=\nabla\vartheta \quad (12)$$

and the curvature (κ) is then the divergence of the unit normal vector:

$$\kappa=\nabla\cdot\frac{n}{|n|}. \quad (13)$$

The volume force acting on each interfacial control volume is then found and is added to the momentum equation as the last term in Eq. (8).

The flow of a bubble in an inclined tube necessitates the introduction of a further complication due to the presence of the tube wall. The wall affects the curvature of the interface for cells near the boundary, and this is modelled by the imposition of a fluid–wall contact angle, ϕ, that is used to adjust the unit normal vector in cells near the wall. The contact angle is not simply a material property of the fluid, but also depends on the smoothness and geometry of the wall and the rate of advance of the interface (Kafka and Dussan, 1979). The choice of this angle will be discussed later.

The 3D momentum, mass continuity, pressure and volume fraction continuity equations were solved iteratively with correction of the pressure field using the SIMPLE algorithm, adapted for non-orthogonal body-fitted coordinates.

4.2. The computational grid

A number of different structured grids based on curvilinear body-fitted coordinates were constructed to solve the five flow equations, in a semi-cylindrical domain used to model the passage of the air bubble up an inclined tube. The coarsest grid used ($251\times21\times11$) is shown in Fig. 5 for a 32 mm diameter tube of 1 m in length. It can be seen that the grid is somewhat non-orthogonal in the 'corners' of the computational domain as a result of using a body-fitted coordinate scheme on a circular geometry. This undesirable grid non-orthogonality or 'skewness' occurs in only very localised regions and is not

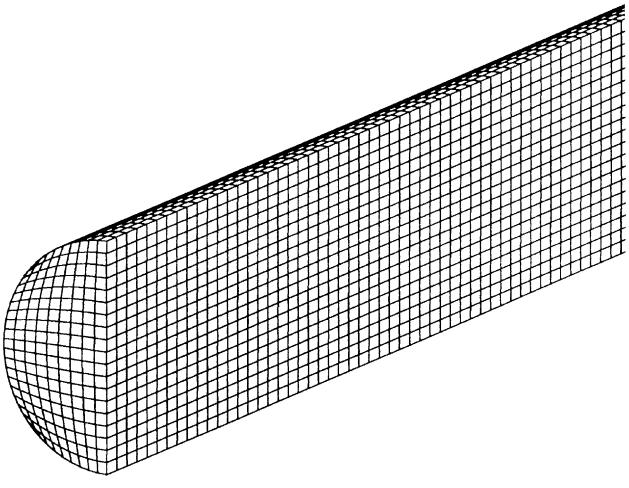

Fig. 5. Isometric view of the coarsest computational grid ($251\times21\times11$).

expected to have any adverse effect on the solution. Nonetheless, the orthogonality of the grid was maximised by smoothing the grid with an application of the Laplace equation, resulting in interior grid lines that curve and bulge.

The symmetric nature of the problem allowed the tube centre to be modelled as a symmetry boundary and consequently only one half of the tube needed to be modelled. All other boundaries were modelled as stationary walls and no inlet or outlet was necessary.

4.3. Time dependant solution procedure

The desired bubble velocity in a stagnant liquid was obtained by tracking the time dependant evolution of the volume fraction field along the inclined tube. Body forces were applied to the x and y momentum equations to simulate the effect of gravity at the specified angle of inclination, and an initial gas bubble was placed at the bottom of the liquid filled tube by specifying the initial volume fraction field. No attempt was made to specify an accurate initial 3D bubble shape. Rather, a rectangular bubble was placed in the computational domain and the volume fraction field allowed to adjust over time until a terminal bubble speed and shape was reached. The length of the initial bubble was set such that a terminal bubble of about 200 mm in length was produced, and the length of the domain was chosen so the bubble would take about 2 s of simulated time to traverse the tube using a time step of typically 10^{-3} s.

An alternative to this procedure would have been to model the flow in a reference frame that moved with the bubble. This would require an inlet and outlet to be specified and the pipe wall to move at the bubble velocity, thus maintaining the bubble stationary within the tube. This approach was used by Tomiyama et al. (1994) for axisymmetric vertical bubble motion. However, an a priori knowledge of the bubble velocity is required or else several calculations are required to find the correct velocity such that the bubble is held stationary. The approach adopted here required a larger computational domain, however, only one run was required for each case investigated.

4.4. Solution invariance

Before the results of the computations could be compared with the experimental values of bubble rise velocity, a number of checks were made to ensure that the model results were independant of the grid structure and size, the convergence criteria, the time step and the bubble length.

A number of different grids were generated with different grid refinements in each direction, the most refined grid had 500,000 elements, and less than 1% variation was found in the calculated drift velocity. The time step, the residual sum convergence criteria and the bubble length were also varied and again no significant affect on the bubble velocity was found.

Calculations were performed for the laminar flow regime. However, for pipes larger than 44.5 mm, the Reynolds number of the liquid film under the bubble was found to be greater than the laminar-turbulent transition value in single-phase pipe flow. Such relatively high values occurred only in the liquid film and were generally confined to a small region at the rear of the bubble. While such localised turbulence was not expected to affect the overall flow field significantly, one computation was performed in which a turbulence model was employed throughout the flow. In order to model such turbulent flow the grid was altered to ensure that the first computational node away from the wall was within the region necessary to use a standard wall function. The two equation k-ϵ model with standard constant values derived from pipe flow was used, and this added considerable numerical complexity and cost to the computations. Despite this, the turbulent solution was indistinguishable from the laminar case, confirming that any localised turbulence would not alter the calculated bubble velocity.

5. Numerical results

A total of 20 simulations were performed in order to compare the numerically determined bubble speed and shape with the data collected in the 32, 44.5 and 50 mm diameter pipes. Both air–water and air–ethylene glycol fluid combinations were investigated for inclination angles of 5–75° from the horizontal. Additionally, simulations were performed for extreme values of dimensionless surface tension in both a 10.6 mm and a 178.0 mm diameter pipe. These results were compared with data collected for pipes of the same diameter by Zukoski (1966).

Fig. 6 shows the time history of the volume fraction field at the central plane of a 50 mm diameter, 1 m long pipe at 5° angle of inclination. The initial rectangular gas bubble can be seen to quickly develop into a typical bubble shape within about 0.5 s. The speed of the bubble also reached a steady value after about 0.5–1 s had elapsed, and this was found to be true for all the cases investigated. The front of the bubble is well rounded and its shape remained constant as the bubble progressed, while the rear of the bubble consisted of a sloped and undulating interface whose shape changed considerably with time.

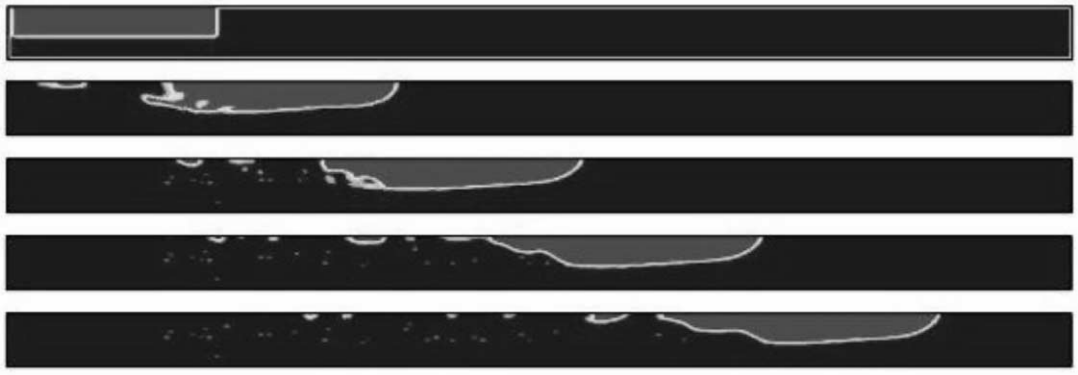

Fig. 6. Evolution of the volume fraction field over a two second interval from top left to bottom right (air–water, $D = 50$ mm, $\beta = 5°$).

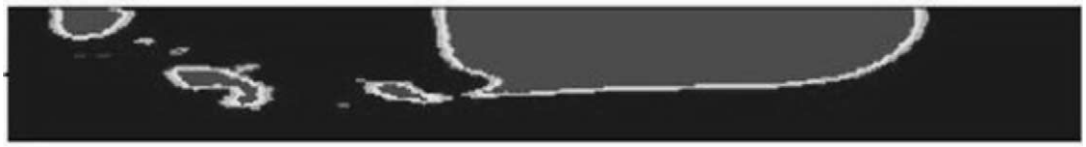

Fig. 7. Numerical result showing bubble shape and entrainment (air–water, $D = 44.5$ mm, $\beta = 45°$).

The shape of the rear of the bubble changed significantly with inclination, becoming more flat and abrupt as the angle of inclination was increased. This effect is shown in Fig. 7 for a bubble at 45° in the 44.5 mm pipe. Interestingly, the abrupt end to the bubble can be seen to induce the ejection of small bubbles from its rear, thus capturing entrainment of dispersed gas in the liquid behind the rising bubble. Sporadic entrainment was observed in the results and was particularly pronounced for highly inclined flows, however, the degree of entrainment was observed to be very grid dependant.

5.1. Dynamic wall contact angle

The only empiricism to be introduced into the numerical scheme involved the choice of the wall contact angle, ϕ. This angle is measured between the interface and the wall within the liquid phase, and visual observations suggest that an acute angle is appropriate as the bubble nose penetrates into the liquid. For a static situation the magnitude of the equilibrium contact angle is a matter of thermodynamics and is ruled by Young's equation (Rillaerts and Joos, 1980). It is known that the contact angle is different from its equilibrium value if the interface moves relative to the solid surface and that both the speed of the interface and the roughness of the wall affect this dynamic contact angle. Many studies have been conducted to measure this quantity, such as those of Kafka and Dussan (1979), however, a search of the literature did not bare any information relevant to the relatively high velocity bubbles investigated here.

A parametric study was performed to investigate the appropriate value of ϕ to employ in the simulations, and the sensitivity of the terminal bubble speed to the value used. Typical results of such a study are shown in Fig. 8, from which two conclusions can be drawn. First, the bubble velocity is not highly sensitive to the value of used, provided an angle is chosen that is not close to the extreme values of 0° or 90°. Second, the best agreement between the predicted and measured bubble rise velocity was achieved with intermediate contact angle values. These findings were found to be true, regardless of the diameter of the pipe being simulated or the inclination angle. Simulations were also compared with the data collected using ethylene glycol as the liquid phase and published data for air–acetone systems, and similar trends were found. As a result of these findings all further simulations were conducted with ϕ set equal to 45°.

5.2. Velocity results

The numerical calculations correctly predicted the variation of the terminal rise velocity of a bubble with inclination angle such that the maximum velocities were attained at inclinations close to 45°. The effect of diameter was also accurately modelled with an increase in diameter leading to an increase in the bubble velocity. Quantitative comparisons between the calculated bubble rising velocity and the data collected in this work as well as the published results of Zukoski (1966) are shown in Fig. 9. It can be seen that very good agreement was obtained for all the pipe diameters from 10.6 to 178 mm. The error in the predicted velocities was generally less than 1% for inclinations less than 30° and the error attained a maximum of about 3–5% for flows at 45°, with the maximum error occurring for the 178 mm diameter simulation at 45°. This result probably occurs because of the spatially coarse grid in the large diameter pipe that may not have been able to accurately capture the sharp curvature of the interface very close to the pipe wall.

The results confirm the feasibility of using the VOF technique to predict bubble velocities in stagnant liquid in inclined pipes with only one empirically determined input, namely the contact angle ϕ.

5.3. Bubble shape

The shape of the phase interface for bubbles in the 32 and 50 mm diameter pipes were measured at the vertical symmetry plane of the pipe using the parallel wire conductance probe.

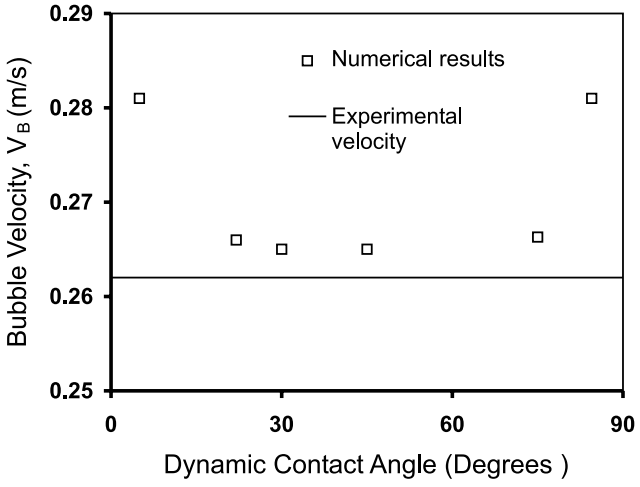

Fig. 8. Typical variation of calculated V_B with wall-contact angle.

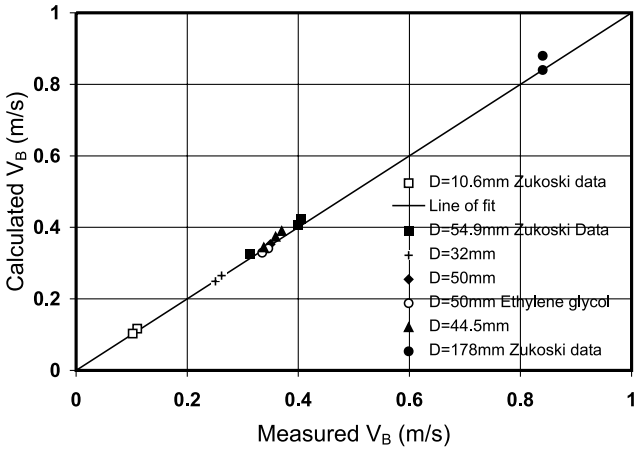

Fig. 9. Comparison of measured and calculated bubble rise velocities.

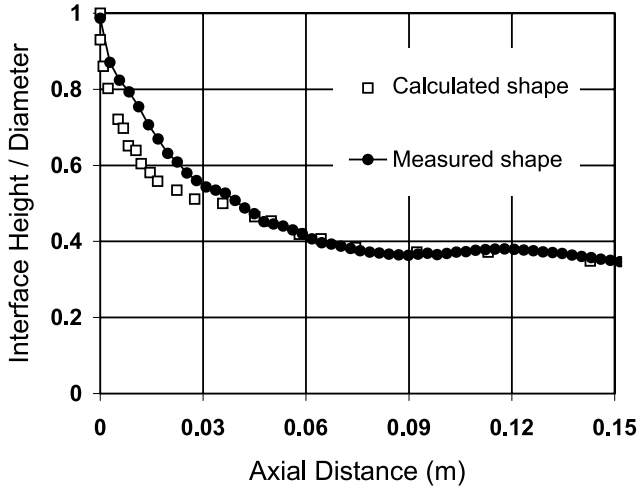

Fig. 10. Comparison of calculated and measured interfacial shape ($D = 32$ mm, $\beta = 10°$).

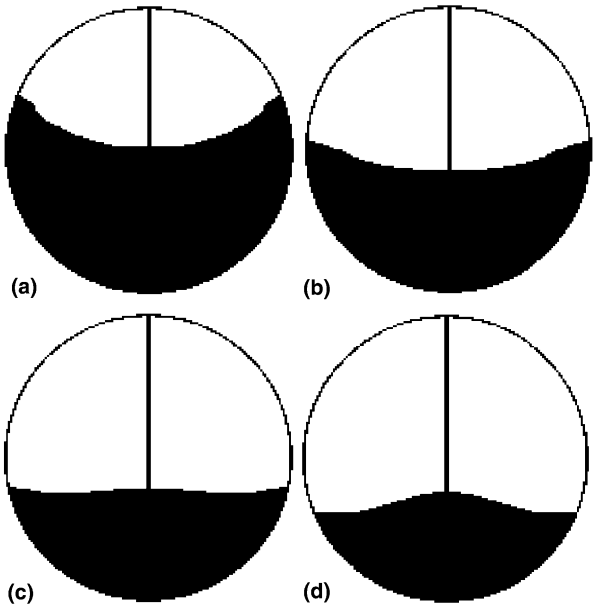

Fig. 11. Progression of transverse interface shape along length of bubble. ($D = 44.5$ mm, $\beta = 45°$).

These measured shapes were compared against the shapes of the bubbles predicted by the numerical calculations and a typical example is shown in Fig. 10. This figure shows that the calculated interface is initially lower than that measured, however, for distances of greater than only about 40 mm aft of the bubble nose, the agreement is good. Generally the agreement between the measured and calculated bubble shapes is reasonably good and improves as the distance along the bubble increases. Fig. 10 also shows waves along the interface that were clearly observable visually, as has also been noted by Fagundes-Netto et al. (1999), and moreover, an alternating pattern of transverse waves could be seen whereby wave crests at the pipe centreline occurred between troughs near the pipe wall. The calculations correctly captured this 3D effect, which is shown in the series of plots comprising Fig. 11. This figure shows that near the nose of the bubble the interface is highly concave, as would be expected. As the distance from the nose is increased, however, the interface flattens and then at about 100 mm back from the bubble nose a convex interface is apparent, whereby the height of the interface is greatest at the centre. Thus a transverse wave pattern is set up that attenuates along the length of the bubble.

Finally, it is interesting to investigate the calculated velocity field shared by both phases, in and around a propagating bubble. The velocity vectors displayed at every third computational cell around a bubble are shown in Fig. 12, and it can be seen that a circulation zone is set-up within the gas bubble. Also the vectors show that the presence of the bubble affects the liquid only a very small distance ahead of it. Notably, a maximum speed of 1.3 m/s was attained in the liquid film, despite a bubble velocity of only about 0.4 m/s.

6. Conclusions

One-dimensional intermittent flow models are highly sensitive to the value of the slug velocity chosen in the calculations, and the data presented shows a transition in this velocity as the flow mixture velocity is increased. A general correlation has been proposed for the slug velocity as well as a transition criterion. Further, it is proposed that this transition, which is produced by a change in the dynamics of the bubble, serves to distinguish between the elongated bubble and the slug flow regimes, and other intermittent flow parameters are shown to dramatically change at this transition point.

The velocity transition is shown to be determined by the value of the speed of a bubble in a stagnant liquid. This important quantity was measured in both a 32 and 50 mm diameter pipe and in a 44.5 mm pipe inclinable up to 90°. The results show the characteristic maximum velocity for inclinations near 45° and agree well with previously published data.

The importance of the bubble drift velocity prompted an attempt to numerically calculate this quantity by simulating the motion of a bubble in a three-dimensional liquid filled tube. The simulations were performed by solving the Navier–Stokes equations on a structured grid and employing the VOF technique to track the gas–liquid interface. Bubble drift velocities were calculated for inclinations from 5° to 75°, and over a wide range of dimensionless surface tensions. Comparison of the calculated results with the data collected both here and from the literature, showed very good agreement for all combinations of tube diameter, surface tension and inclination. The numerical scheme also predicted the bubble shape

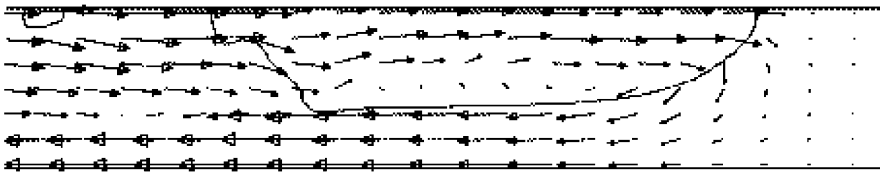

Fig. 12. Calculated velocity distribution. ($D = 44.5$ mm, $\beta = 45°$).

reasonably well and interestingly, captured the undulating nature of the interface under a propagating bubble.

References

Bendiksen, H.K., 1984. An experimental investigation of the motion of long bubbles in inclined tubes. Int. J. Multiphase Flow 10, 467–483.

Benjamin, T.B., 1968. Gravity currents and related phenomena. J. Fluid Mech. 31, 209–248.

Bonnecaze, R.H., Erkine, Jr., Greskovich, E.J., 1971. Holdup and pressure drop for two-phase slug flow in inclined pipelines. AIChE. J. 17, 1109–1113.

Brackbill, J.U., Kothe, D.B., Zemach, C., 1992. A continuum method for modelling surface tension. J. Computat. Phys. 100, 335–354.

Clarke, A., Issa, R.I., 1997. A numerical model of slug flow in vertical tubes. Comput. Fluids 26, 395–415.

Cook, M.C., Behnia, M., 1997. Film profiles behind liquid slugs in gas–liquid pipe flow. AIChE. J. 43, 2180–2186.

Cook, M., Behnia, M., 2000. Slug length prediction in near horizontal gas–liquid intermittent flow. Chem. Eng. Sci. 55, 2009–2018.

Davies, R.M., Taylor, G., 1950. The mechanics of large bubbles rising through extended liquids and through liquids in tubes. Proc. R. Soc. London, Ser. A 200, 375–390.

Dukler, A.E., Hubbard, M.G., 1975. A model for gas–liquid slug flow in horizontal and near horizontal tubes. Ind. Eng. Chem. Fundam. 14, 337–347.

Dumitrescu, D.T., 1943. Stromung an einer luftbase im senkrechten rohr Z. Angew. Math. Mech. 23, 139–149.

Fabre, J., Line, A., 1992. Modeling of two-phase slug flow. Annu. Rev. Fluid Mech. 24, 21–46.

Fagundes-Netto, J.R., Fabre, J., Peresson, 1999. Shape of long bubbles in horizontal slug flow. Int. J. Multiphase Flow 25, 1129–1160.

Ferre, D., 1979. Ecoulements diphasiques a poches en conduit horizontale. Rev. 'Insti. Franca. Pet. 34, 113–142.

Gregory, G.A., Nicholson, M.K., Aziz, K., 1978. Correlation of the liquid volume fraction in the slug for horizontal gas–liquid slug flow. Int. J. Multiphase Flow 4, 33–39.

Heywood, N.I., Richardson, J.F., 1979. Slug flow of air-water mixtures in a horizontal pipe: determination of liquid holdup by γ-ray absorbtion. Chem. Eng. Sci. 34, 17–30.

Hirt, C.W., Nichols, B.D., 1981. Volume of fluid (vof) method for the dynamics of free boundaries. J. Computat. Phys. 39, 201–223.

Kafka, F.Y., Dussan, V.E., 1979. Interpretation of dynamic contact angles in capillaries. J. Fluid Mech. 95, 539–549.

Kokal, S.L., Stanislav, J.F., 1989. An experimental study of two-phase flow in slightly inclined pipes-ii liquid holdup and pressure drop. Chem. Eng. Sci. 44, 681–693.

Mack, K., Bugg, J.D., Rezkallah, K.S., 1997. Numerical simulation of slug flow at zero gravity. In: Gas–Liquid Two-Phase Flows, ASME, 16, Vancouver Summer Meeting.

Mattar, L., Gregory, G.A., 1974. Air-oil slug flow in an upward-inclined pipe – i: slug velocity, holdup and pressure gradient. J. Can. Pet. Technol. 13, 69–77.

Paglianti, A., Giona, M., Soldati, A., 1996. Characterization of subregimes in two-phase slug flow. Int. J. Multiphase Flow 22, 783–796.

Rillaerts, E., Joos, P., 1980. The dynamic contact angle. Chem. Eng. Sci. 35, 883–887.

Rudman, M., 1998. A volume tracking method for incompressible multifluid flows with large density variations. Int. J. Numeric. Methods Fluids 28, 357–378.

Singh, G., Griffith, P., 1970. Determination of the pressure drop optimum pipe size for a two-phase slug flow in an inclined pipe. Trans. ASME, J. Eng. for Ind., 717–725.

Tomiyama, A., Sou, A., Sakaguchi, T., 1994. Numerical simulation of a taylor bubble in a stagnant liquid. ASME Numeric. Method Multiphase Flows 185, 269–276.

Zukoski, E.E., 1966. Influence of viscosity, surface tension, and inclination angle on the motion of long bubbles in closed tubes. J. Fluid Mech. 25, 821–837.